

Article

Experimental Study of the Dynamic Shear Modulus of Saturated Coral Sand under Complex Consolidation Conditions

Weijia Ma ¹, You Qin ² , Fei Gao ¹ and Qi Wu ^{2,*}

¹ School of Mechanical Engineering, Nanjing University of Science and Technology, Nanjing 210094, China

² Institute of Geotechnical Engineering, Nanjing Tech University, Nanjing 210009, China

* Correspondence: qw09061801@163.com

Abstract: The shear modulus is an essential parameter that reflects the mechanical properties of the soil. However, little is known about the shear modulus of coral sand, especially under complex consolidation conditions. In this paper, we present the results of a multi-stage strain-controlled undrained cyclic shear test on saturated coral sand. The influences of several consolidation state parameters: effective mean principal stress (p'_0), consolidation ratio (k_c), consolidation direction angle (α_0), and coefficient of intermediate principal stress (b) on the maximum shear modulus (G_0), the reference shear strain (γ_r) and the reduction of shear modulus (G) have been investigated. For a specified shear strain level, G will increase with increasing p'_0 and k_c , but decrease with increasing α_0 and b . However, the difference between G for various α_0 and b can be reduced by the increase of shear strain amplitude (γ_a). G_0 shows an increasing trend with the increase of p'_0 and k_c ; on the contrary, with the increase of α_0 and b , G_0 shows a decreasing trend. To quantify the effect of consolidation state parameters on G_0 , a new index (μ_{G_0}) with four parameters ($\lambda_1, \lambda_2, \lambda_3, \lambda_4$) which is related to p'_0, k_c, α_0, b is proposed to modify the prediction model of G_0 in literature. Similarly, the values of γ_r under different consolidation conditions are also evaluated comprehensively by the four parameters, and the related index (μ_{γ_r}) is used to predict γ_r for various consolidation state parameters. A new finding is that there is an identical relationship between normalized shear modulus G/G_0 and normalized shear strain γ_a/γ_r for various consolidation state parameters and the Davidenkov model can describe the $G/G_0-\gamma_a/\gamma_r$ curves. By using the prediction model proposed in this paper, an excellent prediction of G can be obtained and the deviation between measured and predicted G is all within $\pm 10\%$.

Keywords: coral sand; dynamic shear modulus; maximum shear modulus; conference shear strain; prediction model of shear modulus



Citation: Ma, W.; Qin, Y.; Gao, F.; Wu, Q. Experimental Study of the Dynamic Shear Modulus of Saturated Coral Sand under Complex Consolidation Conditions. *J. Mar. Sci. Eng.* **2023**, *11*, 214. <https://doi.org/10.3390/jmse11010214>

Academic Editor: Hem Bahadur Motra

Received: 15 December 2022

Revised: 9 January 2023

Accepted: 11 January 2023

Published: 13 January 2023



Copyright: © 2023 by the authors. Licensee MDPI, Basel, Switzerland. This article is an open access article distributed under the terms and conditions of the Creative Commons Attribution (CC BY) license (<https://creativecommons.org/licenses/by/4.0/>).

1. Introduction

Carbonate soils, most commonly calcium carbonate, are usually divided into three categories based on the calcium carbonate (CaCO_3) content: calcareous sand (<50%), siliceous carbonate sand (50–90%), and carbonate sand (>90%) [1]. Carbonate sand, which originates mainly from coral reefs, is referred to as coral sand. Coral sand is mostly distributed in the tropical ocean [2,3] and is the common reclamation material in ocean engineering [4–6]. Due to the special formation progress of coral sand, it has the particles features of intraparticle pores, high friction angle, high compressibility, low hardness, and fragileness at high-stress levels [3,7–11], which makes the mechanical properties of coral sand quite different from those of terrigenous sand.

The marine environment is extremely complex including the complexity of coral sand deposition and the dynamic loadings on a coral sand foundation. Waves, tsunamis, and earthquakes can threaten the stability of the coral sand foundation, and then affect the safety of ocean engineering. So it is vital to explore the undrained dynamic response of saturated coral sand. The maximum shear modulus G_0 and the reduction of shear modulus (G/G_0) from small to large strain range are the essential parameters in seismic response

analysis studies. Many researchers have studied the dynamic shear modulus of silica sand. The maximum shear modulus G_0 is referred to as the shear modulus at small strain ($\gamma_a < 10^{-6}$), which is a key parameter in the prediction of G . The previous researches reveal that the value of G_0 is related to the void ratio e and the effective confining pressure σ'_0 [12–16]. The void ratio reflects the influence of soil property on G_0 , and the effective confining pressure characterizes the effect of consolidation condition on G_0 . Hara et al. [17] obtained the G_0 of cohesive soils by using shear wave velocity V_s in laboratory and in situ tests ($G_0 = \rho V_s^2$), and a unique correlation is established between G_0 and shear strength S_u . Hardin and Kalinski [18] investigate the shear modulus of gravelly soils including uniform and graded crushed limestone gravel, graded river gravel, standard Ottawa and crushed limestone sands, and gravel–sand–silt mixtures. The modified three-dimensional constitutive equations for the elasticity of particulate materials are used to evaluate G_0 for various types of soils. Goudarzy et al. [19,20] explored the effect of the non-plastic fines content of granular on the maximum shear modulus. The G_0 of clean Hostun sand and Hostun sand mixed with 5%, 10%, 20%, 30%, and 40% fines are analyzed. To evaluate the influence of fine content on G_0 , the equivalent void ratio (e^*) is introduced to replace e in the Hardin model. The modified model has a good prediction for the Hostun sand. Yan et al. [21] investigated the small-strain shear modulus of unsaturated silty-fine sand. They find that there exists an optimum saturation $(S_r)_{opt}$ in silty-fine sand. G_0 reaches its maximum value when the silty-fine sand is in optimum saturation and an improved prediction model for G_0 is proposed for sand under different saturation degrees.

Iwasaki et al. [22] evaluated the degree of shear modulus reduction by using two types of equipment. The test results show that the shear modulus at 10^{-4} shear strain amplitude measured by different equipment is identical, and a simplified procedure for prediction G is proposed. Lanzo et al. [23] reported the test results of two reconstituted grains of sand and three laboratory-made clays. The results indicated that with the increase of σ'_0 and the over-consolidation ratio (OCR), the normalized shear modulus reduction curve ($G/G_0-\gamma_a$) generally increases. Furthermore, with the increase of plasticity index (PI), the effect of σ'_0 , and OCR on shear modulus reduction become small. Senerakis et al. [24] found that the $G/G_0-\gamma_a$ of volcanic sands were more linear than those of quartz sands. This trend was more pronounced at lower σ'_0 and at higher values of the coefficient of uniformity (C_u). The parameters of σ'_0 and C_u may not be used in the modified hyperbolic model to quantify the rate of modulus reduction, and it is probably due to the unique fabric of volcanic sands. Chen et al. [25] investigated the characteristics of shear modulus reduction under isotropic and anisotropic consolidations for silt. The correlations between G/G_0 and γ_a for various complex stress conditions are distinct. However, the correlation between G/G_0 and γ_a/γ_r is identical regardless of the consolidation state parameters.

In recent years, with the rise of ocean engineering, the mechanical properties of coral sand become the research focus in marine geotechnical engineering. Controlling the quality of hydraulic filling materials is the key to ensuring the construction safety of marine structures [6]. For soil mass, the shear strength is always the most critical mechanical parameter. Many studies have confirmed that the particle size and confining pressure can affect the shear strength of coral sand [26,27]. However, these researchers focused on the shear characteristics of soils under monotonic shear. Since large-scale deformation of saturated coral sand has been observed in the 1993 Mw 7.7 Guam earthquake [28], the 2006 Mw 6.7 and Mw 6.0 Hawaii earthquakes [29], and the 2010 Mw 7.0 Haiti earthquake [30], the dynamic characteristics of coral sand foundation also need further discuss, and the dynamic shear modulus of coral sand is the most essential, which can establish the constitutive relation and guide the construction of offshore engineering. In fact, engineers have long been concerned about the maximum shear modulus together with the dynamic shear modulus reduction of coral sand foundations. Giang et al. [31] found that particle shapes could affect G_0 . Due to the unique particle characteristics of coral sand, the G_0 of coral sand is much higher than that of silica sand. The previous prediction model will underestimate or overestimate the G_0 of coral sand. Chen et al. [32] carried out different types of strain-controlled undrained

cyclic triaxial tests, and a correlation-function-based method is proposed to calculate the secant shear modulus, which shows a good prediction of shear modulus attenuation. Wu et al. [5] studied the dynamic shear modulus of saturated marine coral sand with different fines contents (FC) and relative densities (D_r). To quantify the influence of both parameters mentioned above, the equivalent skeleton void ratio e^*_{sk} is introduced, and a unique correlation can be observed between G_0 , σ'_0 , and e^*_{sk} . However, most of these studies focused on the effect of soil properties such as confining pressure, relative density, void ratio, and coefficient of uniformity on the shear modulus of coral sand. The mechanism of the effect of consolidation state parameters on the shear modulus reduction is still unclear.

In this paper, we present a comprehensive experimental study of the maximum shear modulus and the reduction of the shear modulus with increasing shear strain. The influence of effective mean principal stress (p'_0), consolidation ratio (k_c), consolidation direction angle (α_0), and coefficient of intermediate principal stress (b) on the shear modulus of coral sand is systematically investigated. The cyclic deformation characteristics of the specimens are also analyzed. The cyclic deformation properties of the specimens were also analyzed. The conclusions drawn in this study can lead to a better understanding of the undrained cyclic behavior of saturated coral sand and provide some key parameters for the analysis of the seismic response of coral sand foundations.

2. Test Materials and Apparatus

2.1. Test Material

The tested coral sand material is sourced from the Nansha Islands, South China Sea. Figure 1 shows the particle distribution curve, photograph, and scanning electron microscope (SEM) picture of tested coral sand. The particle shape of the tested coral sand varies from long strips to round, and some coral and marine fragments can also be observed. From a micro perspective (the SEM picture), the tested coral sand particles have rough surfaces and are attached to fine particles. The specific gravity (G_s) of coral sand is 2.80, maximum and minimum void ratio (e_{max} , e_{min}) is 1.72 and 0.99 respectively, according to the ASTM standards of D4253-14 and D4254-14 [33,34]. Since the maximum particle size used in the specimen cannot be greater than 1/6 to 1/7 of the specimen diameter, the maximum particle size of coral sand used in this test is 2 mm. For the particle distribution curve used in this test, the mean particle size (d_{50}) is 0.31 mm, coefficient of uniformity (C_u) and curvature coefficient (C_c) is 4.67 and 0.86 respectively. Following the Unified Soil Classification System [35], the tested coral sand is classified as poorly graded sand (SP).

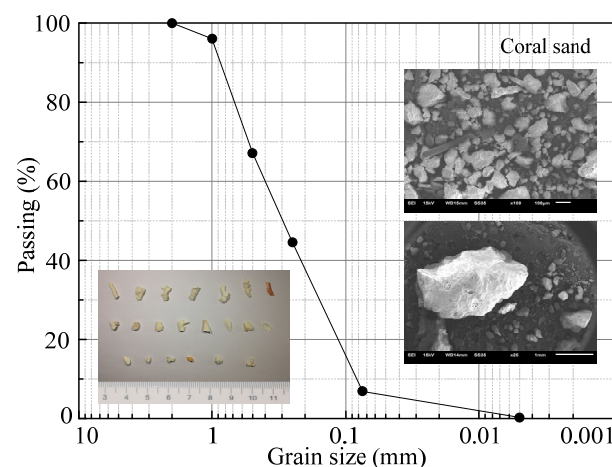


Figure 1. Particle distribution curve, photograph and scanning electron microscope picture (SEM) of tested coral sand.

2.2. Test Apparatus and Stress Distribution

An advanced hollow cylinder torsional shear apparatus manufactured by GDS Instruments (Hook, Hampshire, United Kingdom) is used in this study [Figure 2a]. The

instrument is composed of four parts: pressure chamber, host, pressure controller, and data acquisition system. This apparatus can dynamically and independently control the axial load (W), torque (M_T), outer cell pressure (p_o), and inner cell pressure (p_i). The distributions of these four cyclic loadings on the specimen are shown in Figure 2b. Table 1 gives the performance parameters of the GDS apparatus including the capacity, deviation, and precision of the sensors. The four corresponding stress components (vertical stress σ_z , radial stress σ_r , circumferential stress σ_θ , and torsional shear stress $\tau_{z\theta}$) and three principal stresses ($\sigma_1, \sigma_2, \sigma_3$) are illustrated in Figure 2c,d. Table 2 gives the equations of data interpretation for all consolidation loadings, the stress components, and the consolidation state parameters. More details about this apparatus can be found in the literature [25,36,37].

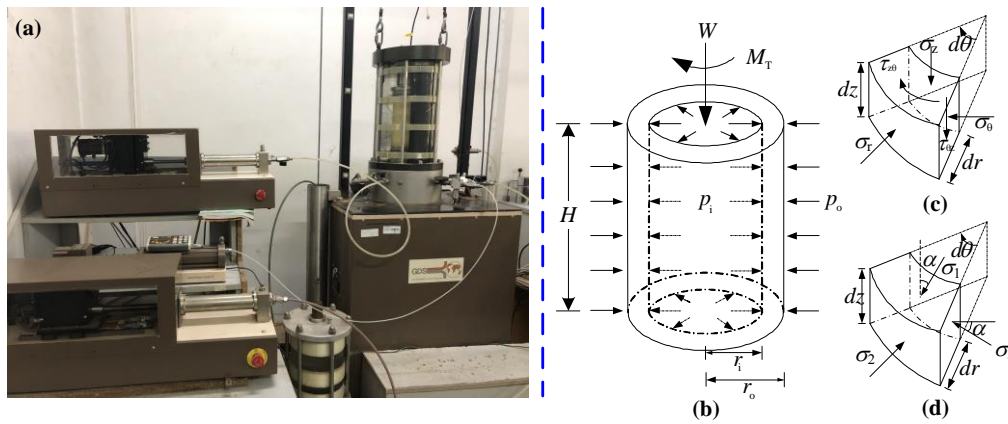


Figure 2. Hollow cylinder apparatus and illustrative stress state in a hollow cylindrical specimen subjected to axial load W , torque M_T , inner pressure p_i , and outer pressure p_o : (a) applied loads, (b) stress components, (c) principal stress components, and (d) major, intermediate, minor principal stress.

Table 1. Performance indexes of the apparatus used in this study.

Controller	Capacity	Deviation	Precision
Axial load	3 kN	0.1% F.S	3 N
Axial displacement	± 40 mm	0.1% F.S	1 μ m
Torque	30 Nm	0.1% F.S	0.03 Nm
Rotation displacement	360°	0.057% F.S	0.04°
Axial/Rotation frequency	≤ 5 Hz	-	-
Outer/inner cell pressure	1 MPa	0.1% F.S	1 kPa
Outer/inner cell volume	200 mL	0.25% F.S	0.001 mL
Back pressure	1 MPa	0.1% F.S	1 kPa
Back volume	200 mL	0.1% F.S	0.001 mL
Pore pressure	1 MPa	0.1% F.S	1 kPa

F.S = full scale.

Table 2. Equations for data interpretation.

Stress Component	Principal Stress	Stress Characteristic Parameter
Vertical $\sigma_z = \frac{W}{\pi(r_o^2 - r_i^2)} + \frac{p_o r_o^2 - p_i r_i^2}{(r_o^2 - r_i^2)}$	Major $\sigma_1 = \frac{\sigma_z + \sigma_\theta}{2} + \sqrt{\left(\frac{\sigma_z - \sigma_\theta}{2}\right)^2 + \tau_{z\theta}^2}$	Mean principal stress $p = \frac{\sigma_1 + \sigma_2 + \sigma_3}{3}$
Radial $\sigma_r = \frac{p_o r_o + p_i r_i}{r_o + r_i}$	Intermediate principal $\sigma_2 = \sigma_r$	Ratio of major and minor principal stress $k_c = \sigma_1 / \sigma_3$
Circumferential $\sigma_\theta = \frac{p_o r_o - p_i r_i}{r_o - r_i}$	Minor principal $\sigma_3 = \frac{\sigma_z + \sigma_\theta}{2} - \sqrt{\left(\frac{\sigma_z - \sigma_\theta}{2}\right)^2 + \tau_{z\theta}^2}$	Coefficient of intermediate principal stress $b = (\sigma_2 - \sigma_3) / (\sigma_1 - \sigma_3)$
Shear $\tau_{z\theta} = \frac{3M_T}{2\pi(r_o^3 - r_i^3)}$		Direction angle of principal stress $\alpha = \frac{1}{2} \arctan\left(\frac{2\tau_{z\theta}}{\sigma_2 - \sigma_\theta}\right)$

3. Specimen Preparation, Saturation, and Consolidation

The hollow cylinder specimen in this study has a height of 200 mm and an inner and outer diameter of 60 mm and 100 mm. The specimen preparation method can significantly affect the mechanical properties of soil [38,39]. To ensure the uniformity of each specimen, the dry deposition method was adopted for preparing the coral sand specimens. The specimens were prepared by pouring the dried sand in seven layers into the hollow space between two molds via a funnel with a near-zero falling head. To investigate the influence of consolidation characteristic parameters on the dynamic shear modulus, the target initial relative density (D_r) of each specimen is 45%, and the corresponding void ratio is 1.355. The actual relative density after consolidation (D_{rc}) for all specimens ranged from 49.18% to 52.88% (see Table 3), and the corresponding void ratio ranged from 1.334 to 1.361. Note that the difference in the relative density before and after the consolidation is about 5%. It is probably due to the high compressibility of coral sand.

Table 3. Scheme of multi-stage strain-controlled undrained cyclic shear tests.

Test No.	End of Consolidation				Soil Property		Test Result		Fitting Parameter	
	p'_0 (kPa)	k_c	α_c (°)	b	D_{rc} (%)	e	G_0 (MPa)	γ_r ($\times 10^{-4}$)	C_1	C_2
01	50	1.0	-	-	49.18	1.361	51.6	5.464	0.46	0.92
02	100				49.45	1.359	68.1	6.056	0.48	0.98
03	200				51.64	1.343	101.1	11.844	0.48	1.02
04	300				52.47	1.337	121.7	15.264	0.48	1.01
05	100	1.5	0	0	50.96	1.348	88.1	8.758	0.52	0.98
06		2.0			51.51	1.344	91.2	12.671	0.52	1.00
07		2.5			52.88	1.334	93.7	14.613	0.52	1.01
08	100	1.5	30		51.37	1.345	82.3	9.497	0.49	1.01
09			45		51.78	1.342	75.6	9.731	0.52	1.04
10			60		51.64	1.343	74.3	10.396	0.50	1.04
11			90		51.51	1.344	66.3	11.650	0.50	1.00
12	100	1.5	0	0.25	51.78	1.342	84.2	9.315	0.47	1.02
13				0.50	51.37	1.345	81.8	9.913	0.52	0.98
14				0.75	51.64	1.343	77.5	10.582	0.49	1.05
15				1.00	51.37	1.345	75.2	11.874	0.50	0.96

After the specimen preparation was complete, the specimen was carefully set in the pressure chamber. The combination method of flushing CO₂ and de-aired water was used to make the specimen attain preliminary saturation, then applying back pressure (p_b) to 400 kPa in three steps (end of step I: $p_b = 100$ kPa, $p_o = p_i = 110$ kPa; end of step II: $p_b = 200$ kPa, $p_o = p_i = 210$ kPa; end of step III: $p_b = 400$ kPa, $p_o = p_i = 410$ kPa); until the Skempton's B-value ≥ 0.97 , which is a criterion indicating the specimen is completely saturated. The effective stress of the specimen always remains at 10 kPa during the saturation. After saturation, the specimens were firstly isotropically consolidated under different effective mean principal stress p'_0 (50, 100, 200, 300 kPa), and then anisotropically consolidated according to the scheme under various consolidation ratios of major and minor principal stress k_c (1.0, 1.5, 2.0, 2.5), direction angle of principal stress α_0 (0°, 30°, 45°, 60°, 90°) and coefficient of intermediate principal stress b (0, 0.25, 0.5, 0.75, 1.0). The whole consolidation process lasts for several hours. When the strain components and back pressure volume are stable, the coral sand specimen can be considered wholly consolidated. The consolidation stress paths are shown in Figure 3. The values of W , M_T , p_o , and p_i for each consolidation condition are illustrated in Table 3. The saturation and consolidation for all the tested specimens were performed following the procedures in the ASTM standard [40].

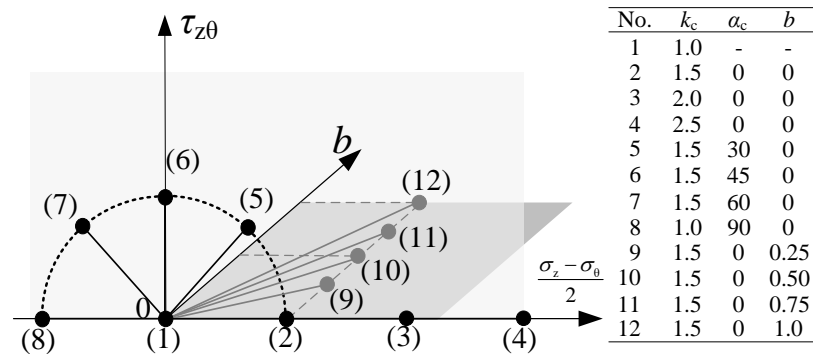


Figure 3. Consolidation stress paths.

4. Multi-Stage Strain-Controlled Undrained Cyclic Shear Tests

It should be noted that under high-frequency seismic load, the saturated sand will generate excess pore water pressure, which will lead to the reduction of effective stress and the destruction of the foundation. In order to truly simulate the dynamic response of saturated coral sand under seismic load in the marine environment, it is more reasonable to choose the undrained test in this study. For each consolidation condition, multi-stage strain-controlled undrained cyclic torsional shear tests were performed. Table 3 lists the detailed procedure for the strain-controlled undrained cyclic shear test. 17 to 20 stages of sinusoidal cyclic strain were applied to each specimen, with ten cycles per stage. ASTM D5311/D5311M standard recommended that a range of cyclic loading frequency $f = 0.1\text{--}2.0$ Hz, and the frequency of 1.0 Hz is preferred [40]. Moreover, many previous studies also used a 1.0 Hz sinusoidal wave as the cyclic loading condition to observe the dynamic response of soil under earthquake events [41–43]. So, the cyclic loading frequency of 1.0 Hz was adopted for all tests in this study to simulate the seismic load. The torsional strain amplitudes change from small strain (0.001%) to large strain (0.5%). After each cyclic loading phase, the specimen was reconsolidated to the initial stress state for 10 min. This stage is intended to dissipate the excess pore water pressure (EPWP) at a large shear strain, which could affect the test result of the next stage [44]. During the drained re-consolidation stage, the volume of the specimen decreased, leading to a slight increase in D_r . However, the value of G can be less affected by density for multi-stage cyclic loading, which has been confirmed in literature [41,45]. Efforts have been made during the whole experiment process to ensure the consistency of the specimen to the greatest extent.

5. Test Results and Analysis

5.1. Typical Results of The Strain-Controlled Test

Figure 4 shows the typical test result of strain-controlled undrained cyclic torsional shear (No. 01). As the number of stages increases, the shear strain amplitude (γ_a) and shear stress amplitude (τ_a) also increase slowly, but not significantly. When γ_a reaches 1×10^{-4} , the shear stress has an observable development; when the strain reaches 2.89×10^{-4} , the EPWP (u_e) starts to develop significantly (more than 2 kPa). Note that the test is strain-controlled, τ_a for each cycle stage is constant and can eventually return to the origin. However, the cyclic shear stress may decrease during the cycle stage and produce deviation in the end. Figure 4d(I) depicts the development of the shear stress-strain relationship in the strain-controlled undrained cyclic shear test. With the increase of shear strain magnitude γ_a , the area of the hysteresis loop becomes large, indicating the gradual decrease in shear strength of the coral sand specimen. Figure 4d(II–IV) is the stress-strain relationship corresponding to the shear strain magnitude of 5×10^{-5} , 5×10^{-4} , and 5×10^{-3} , respectively. The nonlinear of the stress-strain relationship becomes obvious with the increase of γ_a , and the shear stress amplitude gradually decreases at large γ_a . This is because a large strain amplitude causes the EPWP of the coral sand specimen to rise and then increase the flow properties of the soil.

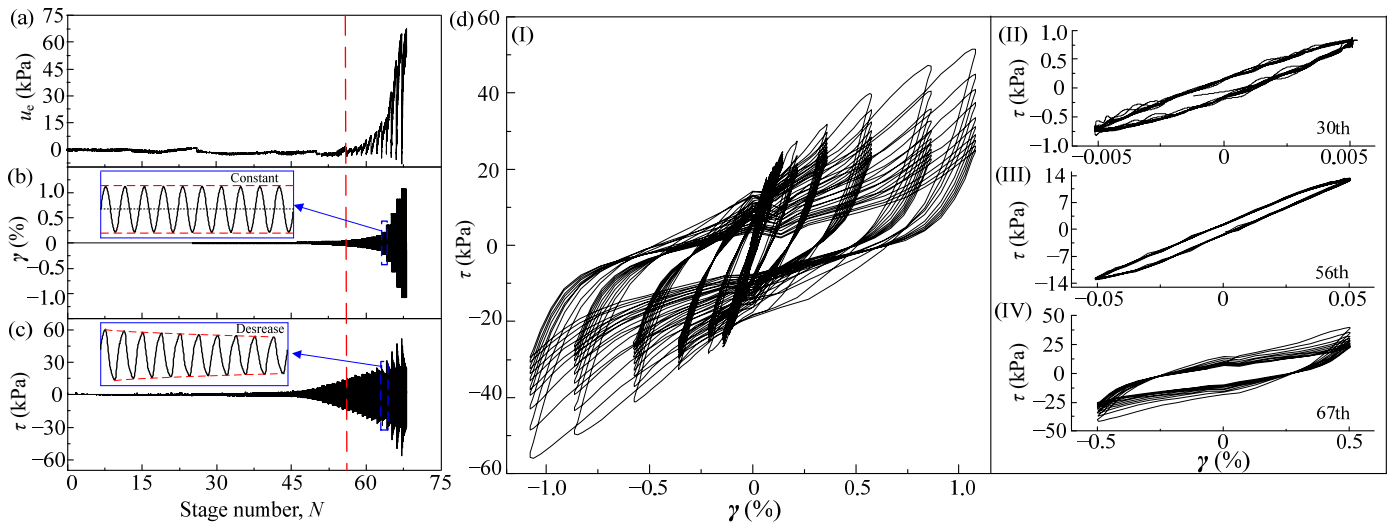


Figure 4. Typical test results of strain-controlled undrained cyclic torsional shear: (a) EPWP (u_e), (b) shear strain (γ), (c) torsional shear stress (τ) along with stage number (N); (d) stress-strain relationship of whole test period and single step.

Figure 5 demonstrates the idealized shear stress-strain response of soil under cyclic torsional shear loading. The strain-dependent secant shear modulus is used to study the modulus attenuation of coral sand in this test, which is commonly used in previous studies.

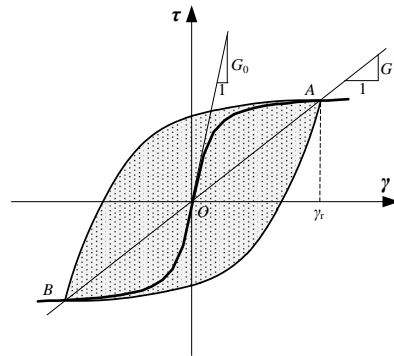


Figure 5. The idealized shear stress-strain response of soil under cyclic loading.

5.2. The Characteristics of Dynamic Shear Modulus under Various Consolidation Conditions

Figure 6 presents the relationship between G and γ_a of saturated isotropically and anisotropically consolidated coral sand for the undrained cyclic torsional shear tests. Clearly, G decreases with the increase of γ_a for all tests, and various consolidation state parameters (p'_0, k_c, α_0, b) have different effects on shear modulus reduction. Under isotropic consolidation, G increases with increasing p'_0 for a specified shear strain level, and the rates of shear modulus reduction for various p'_0 are almost the same. This is consistent with the test result of Kokusho [13] for Toyoura sand and Chen et al. [25] for Nanjing fine sand. However, under anisotropic consolidation, the effect of $k_c, \alpha_0,$ and b on the shear modulus reduction shows different regular. When other parameters (p'_0, α_0, b) are constant, G increases with the increase of k_c . Note that with the increase of k_c , the difference between G becomes small. This can be assumed that when $k_c > 1.0$, the void between coral sand particles begin to decrease gradually, which leads to the rearrangement of particles and the increase of friction between particles, making the shear modulus of coral sand increase significantly. However, when k_c continues to increase, the rearrangement between particles becomes more and more difficult, and the static shear stress only increases the friction between particles. As a result, the differences between the shear modulus for the various

k_c become small as the k_c continues to increase. Yuan et al. (2005) and Sun et al. (2013) obtained similar test results on silt, silty clay, and sludgy soil. They also proposed a prediction model to describe the trend of G_0 with the increase of k_c . [46,47] On the contrary, when α_0 and b increase, the shear modulus for a specified shear strain level shows a decreasing trend. However, this gap becomes smaller as the shear strain increases. When shear strain is over 6×10^{-4} , there is no obvious difference of G value under various α_0 or b . Figure 6 also illustrates the relationship between G and γ_a of saturated Nanjing fine sand under similar consolidation conditions, which is shown in gray symbols. The physical properties of this sandy soil can be found in Chen (2016). It is clear that the regular shear modulus reduction is quite similar for both sandy soils. However, the development trend of the shear modulus for Nanjing fine sand is significantly lower than that for coral sand under the same k_c, α_0, b . However, for the same p'_0 , the modulus attenuation trend of the two sandy soils is quite close.

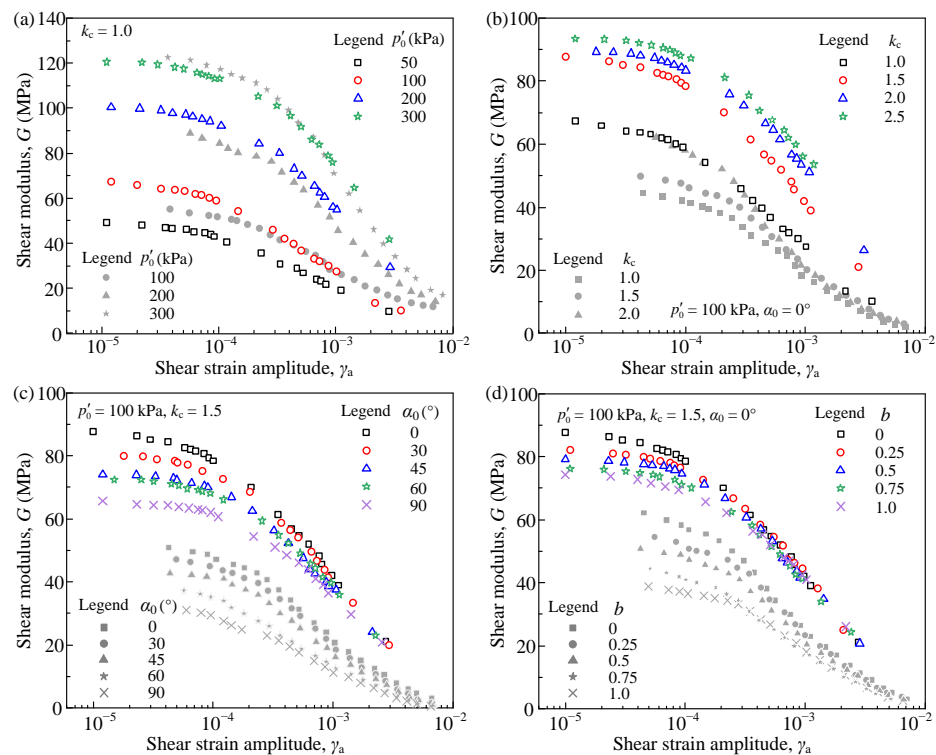


Figure 6. G versus γ_a curves of isotropically and anisotropically consolidated saturated coral sand for the undrained cyclic torsional shear tests under various (a) effective mean principal stress, (b) consolidation ratio, (c) consolidation direction angle, and (d) coefficient of intermediate principal stress.

5.3. The Maximum Dynamic Shear Modulus under Various Consolidation Conditions

The maximum dynamic shear modulus G_0 is an essential parameter in the undrained dynamic shear response of saturated sandy soils. G_0 is generally considered as the shear modulus at a small strain (less than 10^{-6}). To investigate the correlation between G_0 and various consolidation state parameters, a total of 15 strain-controlled undrained cyclic torsional shear tests were performed using the GDS hollow cylinder apparatus. Due to the limited testing accuracy of this apparatus, the dynamic shear modulus less than 1×10^{-5} is hardly measured, and G_0 cannot be obtained directly. However, according to the hyperbolic model proposed by Hardin and Drnevich [48], G_0 can be calculated by

$$G_0 = \lim_{\gamma \rightarrow 0} \frac{1}{a_1 + b_1 \gamma}, \tag{1}$$

where a_1 and b_1 are the linear fitting parameter. Hardin also gives the model to predict the G_0 of sandy soils:

$$G_0 = AF(e) \left(\frac{\sigma'_0}{P_a} \right)^n P_a, \tag{2}$$

where A and n are the material parameters, σ'_0 is effective confining pressure in the triaxial test, P_a is the atmospheric pressure ($P_a = 100$ kPa in this study), and $F(e)$ is a function related to void ratio (e). As mentioned above, the consolidation state parameters (p'_0, k_c, α_0, b) have different effects on the dynamic shear modulus, and Equation (2) cannot completely predict G_0 under complex consolidation conditions.

Figure 7 shows the correlations between G_0 and various consolidation parameters. Clearly, with the increase of mean effective principal stress and consolidation ratio, G_0 shows a gradually increasing trend. On contrary, with the increase of consolidation direction angle and coefficient of intermediate principal stress, G_0 shows a decreasing tendency.

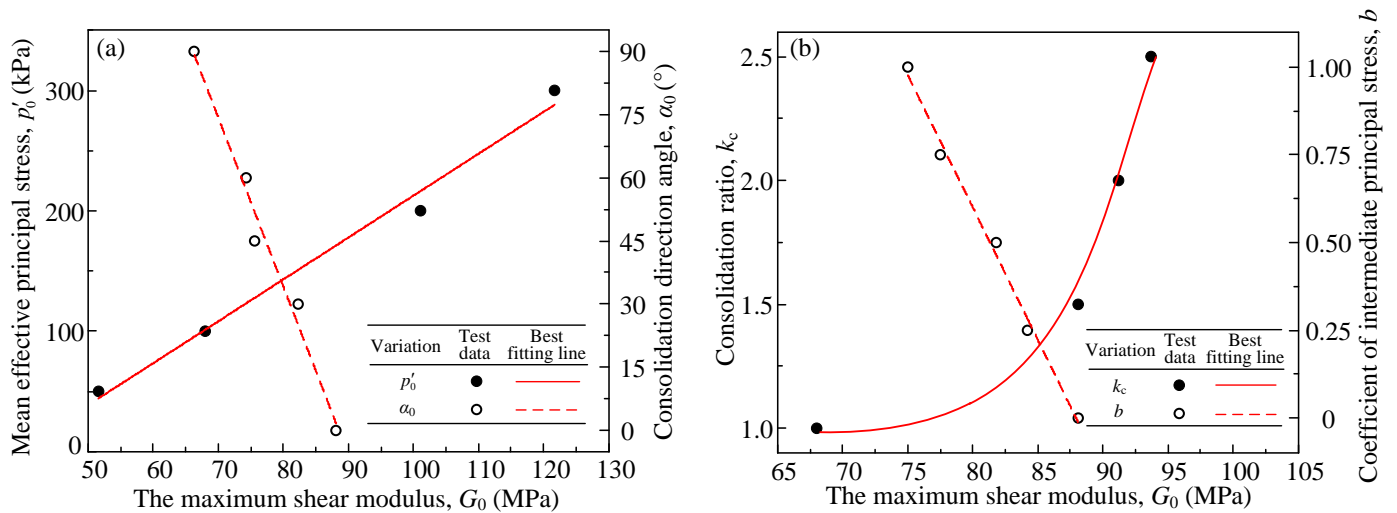


Figure 7. The correlations between the experimental G_0 and various consolidation parameters under various (a) effective mean principal stress and consolidation direction angle, (b) consolidation ratio and coefficient of intermediate principal stress.

To quantify the influence of the above parameters on G_0 , a new index denoted as μ_{G0} is introduced, which can be expressed as follows:

$$\mu_{G0} = \lambda_1^{n_1} \lambda_2^{n_2} \lambda_3^{n_3} \lambda_4^{n_4}, \tag{3}$$

where

$$\lambda_1 = \frac{p'_0}{P_a}, \lambda_2 = k_c, \lambda_3 = \cos\left(\frac{\alpha_0}{2}\right), \lambda_4 = \frac{1}{2+b}$$

and $n_1, n_2, n_3,$ and n_4 are the weights for various parameters. Figure 8 shows the correlation between the measured G_0 and μ_{G0} . For the coral sand in this study, when $n_1 = 0.527, n_2 = 0.419, n_3 = 0.760, n_4 = 0.220$, there is a strong linear relationship between G_0 and μ_{G0} under complex consolidation conditions.

Furthermore, $F(e)$ in Equation (2) can be equal to e^a for simplicity according to the literature [14,16]. Thus, the prediction model of G_0 can be rewritten as:

$$G_0 = Ae^a \mu_{G0} P_a, \tag{4}$$

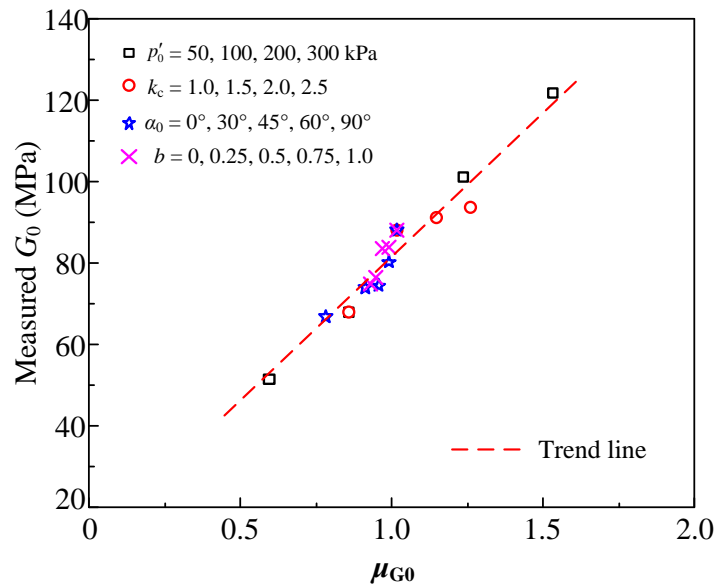


Figure 8. The correlation between the experimental G_0 versus μ_{G_0} .

For the tested coral sand, the appropriate values of A and a are 0.57 and 1.25, respectively. For the isotropic condition, it is difficult to define the value of α_0 and b in hollow cylinder specimens through the calculation equations. Since the σ_2 is always equal to σ_3 in cylinder specimen for the triaxial test, it is reasonable to make $\alpha_0 = 0^\circ$, and $b = 0$ under isotropic conditions. When $n_2 = n_3 = n_4 = 0$ (triaxial test), Equation (4) degenerates to Equation (2). The predicted G_0 for various consolidation conditions by using Equations (3) and (4) are illustrated in Table 3. Figure 9a shows the comparison between the measured and predicted G_0 of saturated coral sand. It is striking to find that all the test data are close to the line of $y = x$, within $\pm 10\%$ deviation, indicating a good prediction of the proposed model on G_0 . The prediction results of Nanjing fine sand are also shown in Figure 9b. When $n_1 = 1.0$, $n_2 = 0.7$, $n_3 = 1.5$, and $n_4 = 0.2$, an acceptable prediction of G_0 within $\pm 20\%$ deviation can be obtained by using Equation (4).

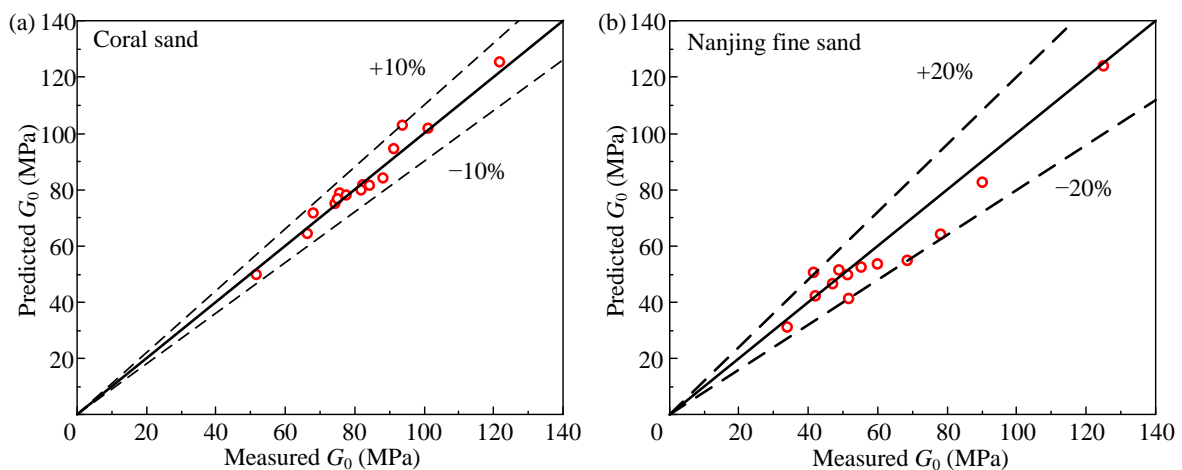


Figure 9. The comparison between the experimental G_0 versus predicted G_0 of (a) coral sand and (b) Nanjing fine sand under various consolidation conditions.

5.4. The Prediction Model of Dynamic Shear Modulus Reduction

Figure 10 shows the relationships between normalized shear modulus G/G_0 and γ_a of saturated isotropically and anisotropically consolidated coral sand. It seems that the G/G_0 versus γ_a curves shift to the right with the increase of p'_0 and k_c . However, with the

increase of α_0 and b , the $G/G_0-\gamma_a$ curves have little change. This implies that the feature of dynamic shear modulus reduction can be significantly affected by p'_0 and k_c , rather than α_0 and b , and the consolidation state parameters of α_0 and b mainly affect the maximum shear modulus of coral sand.

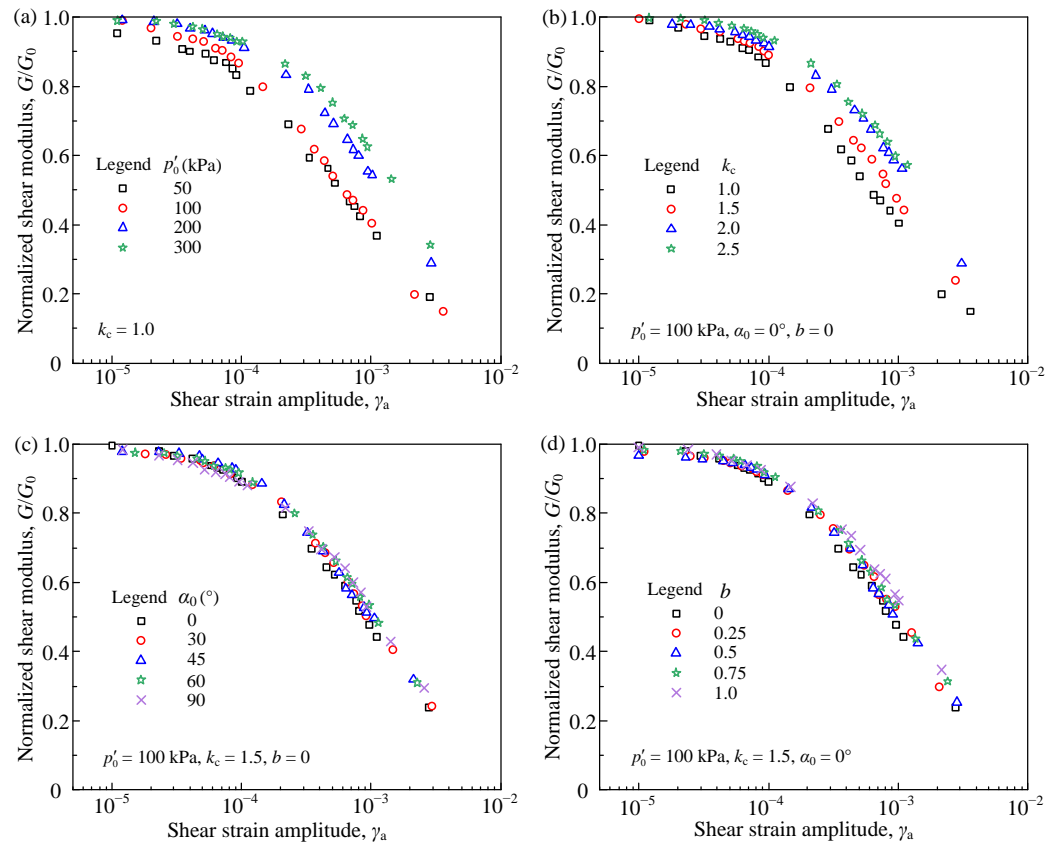


Figure 10. G_0 versus γ_a curves of isotropically and anisotropically consolidated saturated coral sand for the undrained cyclic torsional shear tests under various (a) effective mean principal stress, (b) consolidation ratio, (c) consolidation direction angle, and (d) coefficient of intermediate principal stress.

Figure 11 presents all the test data under various consolidation conditions. The boundaries of dynamic shear modulus for various silica grains of sand in literature are also shown in this figure [12,13,49,50]. The distribution of test data is slightly beyond the upper boundary given by Yuan. This indicates the differences in dynamic mechanical properties between coral sand and silica sand.

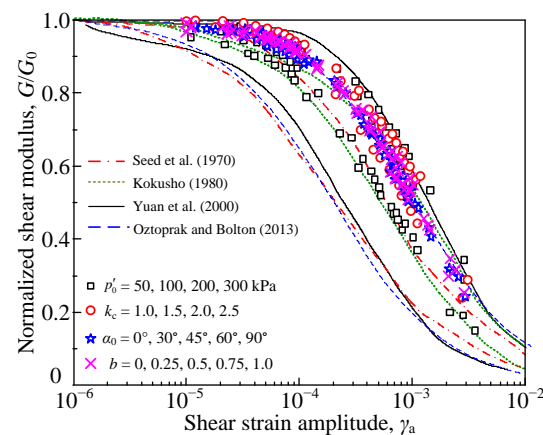


Figure 11. Shear modulus reduction curves of saturated coral sand under various consolidation conditions [12,13,49,50].

The reference shear strain γ_r refers to the value of γ_a corresponding to $G/G_0 = 0.5$, which is a common index to normalize the trend of dynamic shear modulus. Figure 12 plots the normalized shear modulus G/G_0 , and the normalized shear strain γ_a/γ_r curves under various complex consolidation conditions. It is clear to find that the $G/G_0-\gamma_a/\gamma_r$ curves can fall in a very narrow band, indicating the validity of γ_r in characterizing the reduction of dynamic shear modulus. In traditional triaxial tests, the strain-dependent shear modulus reduction can be described by the Davidenkov model [51], which is expressed as

$$\frac{G}{G_0} = 1 - \left[\frac{(\gamma_a/\gamma_r)^{2C_1}}{1 + (\gamma_a/\gamma_r)^{2C_1}} \right]^{C_2}, \tag{5}$$

where C_1 and C_2 are the fitting parameters. The values of C_1 and C_2 for each test are illustrated in Table 3. Since the values of C_1 and C_2 for various consolidation conditions are very close, it is recommended to take the average value of C_1 ($=0.5$) and C_2 ($=1.00$) as the fitting value for all cases. Under these circumstances, Equation (5) degenerates into a hyperbolic model.

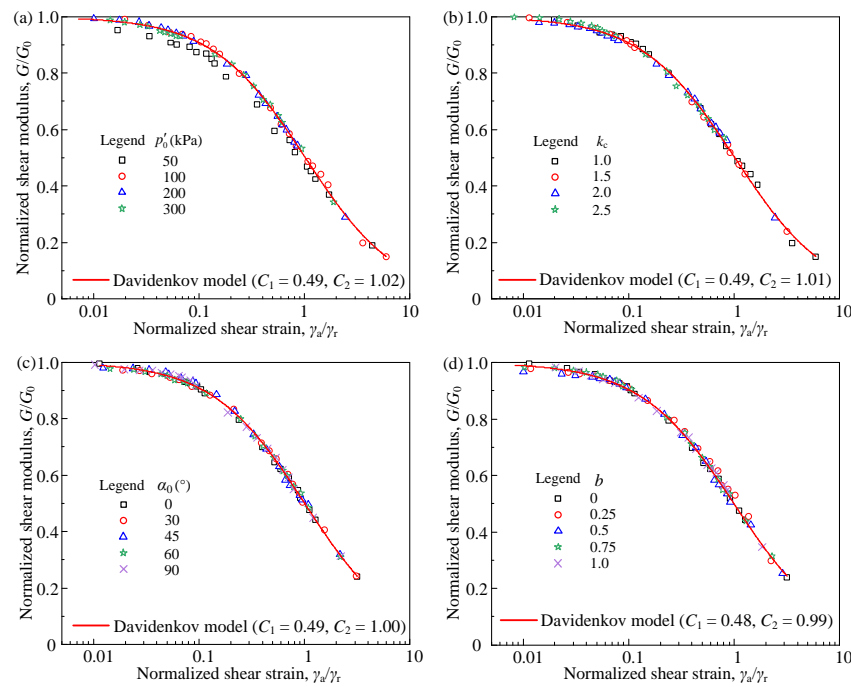


Figure 12. G/G_0 versus γ_a/γ_r curves of isotropically and anisotropically consolidated saturated coral sand for the undrained cyclic torsional shear tests under various (a) effective mean principal stress, (b) consolidation ratio, (c) consolidation direction angle, and (d) coefficient of intermediate principal stress.

It can be seen from the above results that the reference shear strain γ_r is an important parameter that evaluates the trend of shear modulus reduction. Actually, many studies have confirmed that γ_r is related to effective confining pressure σ'_0 and fine content FC . However, the influences of different consolidation state parameters under complex consolidation conditions on γ_r are rarely investigated. Figure 13 shows the correlation between γ_r and four consolidation state parameters (p'_0, k_c, α_0, b). Obviously, when the other three parameters remain constant, the values of γ_r become large with the increase of any one of those parameters. The value of γ_r ranges from 5.464×10^{-4} to 15.264×10^{-4} , and it means the consolidation state parameters affect γ_r to a certain degree. Moreover, compared with α_0 and $b, p'_0,$ and k_c have a greater impact on γ_r .

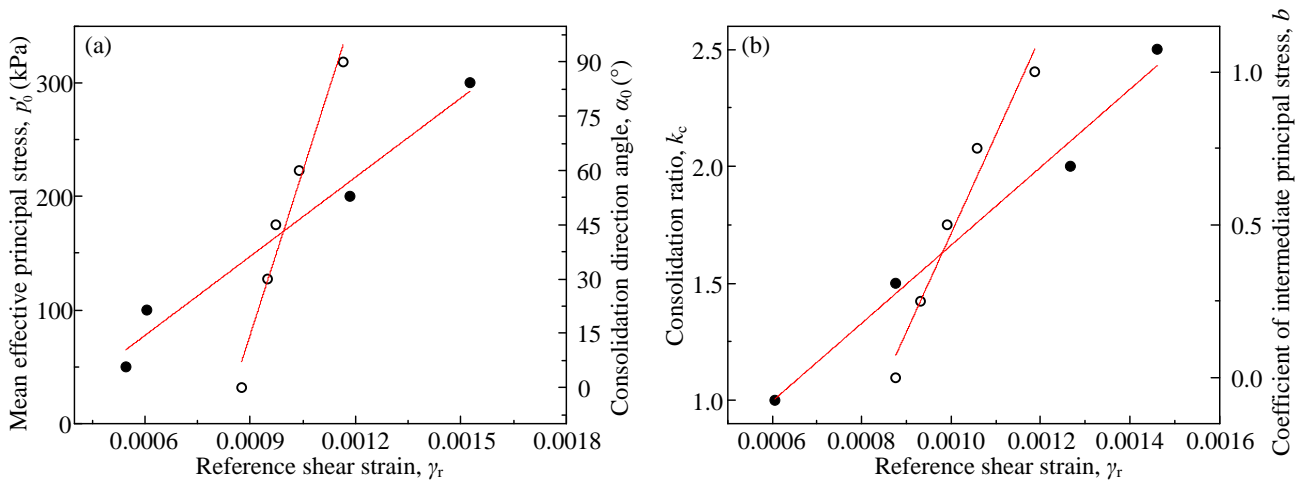


Figure 13. The correlation between γ_r and stress characteristic parameters of (a) effective mean principal stress and consolidation direction angle, (b) consolidation ratio and coefficient of intermediate principal stress.

Similarly, to quantify the influence of different consolidation state parameters on γ_r , another consolidation index μ_{γ_r} is introduced, which can be expressed as follows:

$$\mu_{\gamma_r} = (\lambda_1 \lambda_2) / (\lambda_3 \lambda_4)^m, \tag{6}$$

where $\lambda_1, \lambda_2, \lambda_3,$ and λ_4 have been defined in Equation (3), and m is a calibration parameter that is determined by the correlation between consolidation state parameters and γ_r . Figure 14 shows the correlation between γ_r and μ_{γ_r} . When $m = 1.0$, with the increase of μ_2 , γ_r also presents the increasing tendency, and a strong linear relationship can be found in this figure:

$$\gamma_r = D_1 \times \mu_{\gamma_r} + D_2, \tag{7}$$

where D_1 and D_2 are the linear fitting parameters, and $D_1 = 2.1807 \times 10^{-4}, D_2 = 2.5403 \times 10^{-4}$ for the tested coral sand.

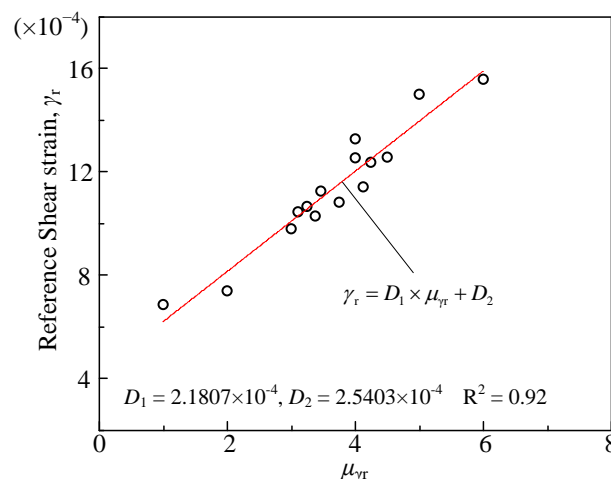


Figure 14. The correlation between reference shear strain γ_r and μ_{γ_r} .

Thus, based on the analysis of the consolidation state parameters, a prediction model of G for an undrained strain-controlled torsional shear test is established by Equations (3)–(7). This new model takes the effective mean principal stress (p'_0), consolidation ratio (k_c), consolidation direction angle (α_0), and coefficient of intermediate principal stress (b) into consideration. To verify the accuracy of the model, Figure 15a shows the correlation between

the measured G in the multi-stage strain-controlled undrained cyclic shear tests and the predicted G calculated from the new model. All data are close to the line of $y = x$, and the deviations of measured and predicted are all within $\pm 15\%$, indicating a good prediction of the proposed new model on G . Figure 15b also shows the prediction result of G for the saturated Nanjing Fine sand, when $m = -1.0$ in Equation (6), a good prediction result can be observed.

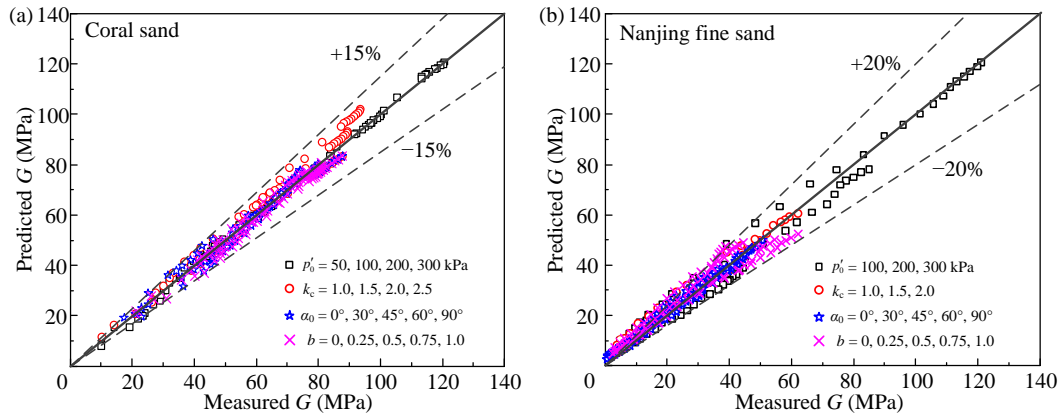


Figure 15. The correlation between the experimental G versus predicted G of (a) coral sand and (b) Nanjing fine sand under various consolidation conditions.

This study provides a comprehensive view of how the consolidation state parameters affect the dynamic shear modulus of saturated coral sand. However, the prediction model proposed in this study is still a semi-empirical formula, which is strongly related to the consolidation state parameters. Due to the lack of test data on the shear modulus under complex consolidation conditions, the correlation between fitting parameters in the formulas and physical properties also needs to be further discussed. More test data are welcomed to verify the applicability of the model and determine the physical meaning of the fitting parameters. According to the existing research results, the next step of the research will focus on determining the physical meaning of the fitting parameters and analyzing the stress state of soil elements to propose a more physical model to better predict the dynamic shear modulus of saturated sand under various consolidation conditions.

6. Conclusions

This study presented results for saturated coral sand from multi-stage strain-controlled undrained cyclic shear tests. The influences of the effective mean principal stress (p'_0), consolidation ratio (k_c), consolidation direction angle (α_0), and coefficient of intermediate principal stress (b) on dynamic shear strain reduction in saturated coral sand are investigated, and the main conclusions are as follows.

1. Shear strain modulus G decreases with the increase of γ_a for all tests, and the consolidation state parameters (p'_0, k_c, α_0, b) have a significant effect on G . For a specified shear strain level, G generally increases with increasing p'_0 and k_c , but decreases with increasing α_0 and b .
2. The consolidation state parameters can affect the maximum shear modulus G_0 severely. Specifically, G_0 has a positive correlation with p'_0 and k_c , and a negative correlation with α_0 and b . This regulation is consistent with that of G . To further analyze the influence of consolidation state parameters on G_0 , a new index (μ_1) that describes the complex consolidation conditions is introduced, and the four parameters $\lambda_1, \lambda_2, \lambda_3, \lambda_4$ in the new index are used to quantify the effect of p'_0, k_c, α_0, b on G_0 , respectively. Based on this index, a new model of G_0 is established, and the test data in this study also proves the validity of this new prediction model.

3. The reference shear strain γ_r under isotropic and anisotropic consolidations are also varied. Based on the parameters of $\lambda_1, \lambda_2, \lambda_3, \lambda_4$, another new index (μ_2) is also proposed, and a strong linear relationship can be observed between γ_r and μ_2 . It is delighted to find that the relationships between normalized shear modulus G/G_0 and normalized shear strain γ_a/γ_r are almost identical. The Davidenkov model can be used to describe the $G/G_0-\gamma_a/\gamma_r$ curves and for simplicity, the recommended parameters of C_1 and C_2 in this model are 0.50 and 1.00, respectively.
4. The prediction model proposed in this paper can well describe the dynamic shear modulus reduction trend of the tested coral sand under isotropic and anisotropic consolidation conditions, and the deviation between measured and predicted G are all within $\pm 10\%$, indicating the good prediction result of this new model. However, due to the lack of test data, more test data is needed to further confirm the effectiveness of the prediction model.
5. The test data in this study can provide important parameters for island reef engineering. Correspondingly, the prediction of dynamic shear moduli with different strains can be a reference for the seismic design of the foundation. Due to the complex consolidation conditions of soils in natural environments, the prediction model of G_0 proposed in this study can be a guideline in engineering practice.

Author Contributions: Conceptualization, W.M. and Q.W.; methodology, W.M.; validation, F.G.; investigation, W.M.; resources, W.M. and Q.W.; data curation, Y.Q.; writing—original draft preparation, W.M.; writing—review and editing, W.M. and Y.Q.; visualization, Y.Q.; supervision, Q.W.; funding acquisition, W.M.; All authors have read and agreed to the published version of the manuscript.

Funding: This research was funded by the National Natural Science Foundation of China (grant number: 52208350).

Institutional Review Board Statement: Not applicable.

Informed Consent Statement: Not applicable.

Data Availability Statement: The data used during the study are available from the first author by request.

Conflicts of Interest: The authors declare no conflict of interest.

References

1. Flores Lopez, F.A.; Taboada, V.M.; Gonzalez Ramirez, Z.X.; Cruz Roque, D.; Barrera Nabor, P.; Dantal, V.S. Normalized modulus reduction and damping ratio curves for Bay of Campeche carbonate Sand. In Proceedings of the Offshore Technology Conference, Houston, TX, USA, 30 April–3 May 2018. [\[CrossRef\]](#)
2. Burke, L.; Reyter, K.; Spalding, M.; Perry, A. *Reefs at Risk Revisited*; Report; World Resources Institute: Washington, DC, USA, 2011.
3. Ma, W.J.; Qin, Y.; Zhao, K.; Chen, G.X. Comparisons on liquefaction behavior of saturated coral sand and quartz sand under principal stress rotation. *Mar. Georesour. Geotechnol.* **2022**, *40*, 235–247. [\[CrossRef\]](#)
4. Liu, L.; Yao, X.; Ji, Z.; Gao, H.; Wang, Z.; Shen, Z. Cyclic behavior of calcareous sand from the South China Sea. *J. Mar. Sci. Eng.* **2021**, *9*, 1014. [\[CrossRef\]](#)
5. Wu, Q.; Liu, Q.F.; Zhuang, H.Y.; Xu, C.S.; Chen, G.X. Experimental investigation of dynamic shear modulus of saturated marine coral sand. *Ocean Eng.* **2022**, *264*, 112412. [\[CrossRef\]](#)
6. Wang, X.Z.; Wang, X.; Shen, J.H.; Ding, H.Z.; Wen, D.S.; Zhu, C.Q.; Lv, S.Z. Foundation filling performance of calcareous soil on coral reefs in the South China Sea. *Appl. Ocean Res.* **2022**, *129*, 103386. [\[CrossRef\]](#)
7. Coop, M.R. The mechanics of uncemented carbonate sands. *Géotechnique* **1990**, *40*, 607–626. [\[CrossRef\]](#)
8. Sharma, S.S.; Ismail, M.A. Monotonic and cyclic behavior of two calcareous soils of different origins. *J. Geotech. Geoenviron. Eng.* **2006**, *132*, 1581–1591. [\[CrossRef\]](#)
9. Brandes, H.G. Simple shear behavior of calcareous and quartz sands. *Geotech. Geol. Eng.* **2011**, *29*, 113–126. [\[CrossRef\]](#)
10. Salem, M.; Elmamlouk, H.; Agaiby, S. Static and cyclic behavior of North Coast calcareous sand in Egypt. *Soil Dyn. Earthq. Eng.* **2013**, *55*, 83–91. [\[CrossRef\]](#)
11. Rui, S.; Guo, Z.; Si, T.; Li, Y. Effect of particle shape on the liquefaction resistance of calcareous sands. *Soil Dyn. Earthq. Eng.* **2020**, *137*, 106302. [\[CrossRef\]](#)
12. Seed, H.B.; Idriss, I.M. *Soil Moduli and Damping Factors for Dynamic Response Analyses*; Report EERC 70-10; University of California: Berkeley, CA, USA, 1970.

13. Kokusho, T. Cyclic triaxial test of dynamic soil properties for wide strain range. *Soils Found.* **1980**, *20*, 45–60. [[CrossRef](#)]
14. Menq, F.Y. Dynamic Properties of Sandy and Gravelly Soils. Ph.D. Thesis, University of Texas at Austin, Austin, TX, USA, 2003.
15. Wichtmann, T.; Triantafyllidis, T. Influence of the grain-size distribution curve of quartz sand on the small strain shear modulus G_{max} . *J. Geotech. Geoenviron. Eng.* **2009**, *135*, 1404–1418. [[CrossRef](#)]
16. Senetakis, K.; Anastasiadis, A.; Ptilakis, K. The small-strain shear modulus and damping ratio of quartz and volcanic sands. *Geotech. Test. J.* **2012**, *35*, 964–980. [[CrossRef](#)]
17. Hara, A.; Ohta, T.; Niwa, M.; Tanaka, S.; Banno, T. Shear modulus and shear strength of cohesive soils. *Soils Found.* **1974**, *14*, 1–12. [[CrossRef](#)] [[PubMed](#)]
18. Hardin, B.O.; Kalinski, M.E. Estimating the Shear Modulus of Gravelly Soils. *J. Geotech. Geoenviron. Eng.* **2005**, *131*, 867–875. [[CrossRef](#)]
19. Goudarzy, M.; Rahman, M.M.; König, D.; Schanz, T. Influence of non-plastic fines content on maximum shear modulus of granular materials. *Soils Found.* **2016**, *56*, 973–983. [[CrossRef](#)]
20. Goudarzy, M.; Rahemi, N.; Rahman, M.M.; Schanz, T. Predicting the maximum shear modulus of sands containing nonplastic fines. *J. Geotech. Geoenviron. Eng.* **2017**, *143*, 0617013. [[CrossRef](#)]
21. Yan, K.; Wang, Y.; Yang, Z.; Lai, X.; Chen, C. Experimental study on small-strain shear modulus of unsaturated silty-fine sand. *Appl. Sci.* **2022**, *12*, 8743. [[CrossRef](#)]
22. Iwasaki, T.; Tatsuoka, F.; Takagi, Y. Shear moduli of sands under cyclic torsional shear loading. *Soils Found.* **1978**, *18*, 39–56. [[CrossRef](#)]
23. Lanzo, G.; Vucetic, M.; Doroudian, T.M. Reduction of shear modulus at small strains in simple shear. *J. Geotech. Geoenviron. Eng.* **1997**, *123*, 1035–1042. [[CrossRef](#)]
24. Senetakis, K.; Anastasiadis, A.; Ptilakis, K. Normalized shear modulus reduction and damping ratio curves of quartz sand and rhyolitic crushed rock. *Soils Found.* **2013**, *53*, 879–893. [[CrossRef](#)]
25. Chen, G.X.; Zhou, Z.L.; Pan, H.; Sun, T.; Li, X.J. The influence of undrained cyclic loading patterns and consolidation states on the deformation features of saturated fine sand over a wide strain range. *Eng. Geol.* **2016**, *204*, 77–93. [[CrossRef](#)]
26. Saeidaskari, J.; Alibolandi, M.; Azizkandi, A.S. Undrained monotonic and cyclic behavior of Qeshm calcareous sand. *Mar. Georesour. Geotechnol.* **2021**, *39*, 798–811. [[CrossRef](#)]
27. Wang, X.; Wang, X.Z.; Shen, J.H.; Zhu, C.Q. Particle size and confining-pressure effects of shear characteristics of coral sand: An experimental study. *Bull. Eng. Geol. Environ.* **2022**, *81*, 97. [[CrossRef](#)]
28. Vahdani, S.; Pyke, R.; Siriprusanan, U. Liquefaction of calcareous sands and lateral spreading experienced in Guam as a result of the 1993 Guam earthquake. In Proceedings of the 5th US—Japan Workshop on Earthquake Resistant Design of Lifeline Facilities and Countermeasures against Soil Liquefaction, Snowbird, UT, USA, 29 September–29 October 1994; pp. 117–134.
29. Chock, G.; Robertson, I.; Nicholson, P.; Brandes, H.; Medley, E.; Okubo, P.; Hirshorn, B.; Sumada, J.; Kindred, T.; Iinuma, G.; et al. *Compilation of Observations of the October 15, 2006 Kiholo bay (Mw 6.7) and Mahukona (Mw 6.0) Earthquakes, Hawai'i*; Report 31; Earthquake Engineering Research Institute (EERI): Oakland, CA, USA, 2006.
30. Olson, S.M.; Green, R.A.; Lasley, S.; Martin, N.; Cox, B.R.; Rathje, E.; Bachhuber, J.; French, J. Documenting liquefaction and lateral spreading triggered by the 12 January 2010 Haiti earthquake. *Earthq. Spectra* **2011**, *27*, 93–116. [[CrossRef](#)]
31. Giang, P.H.H.; Van Impe, P.O.; Van Impe, W.F.; Menge, P.; Haegeman, W. Small-strain shear modulus of calcareous sand and its dependence on particle characteristics and gradation. *Soil Dyn. Earthq. Eng.* **2017**, *100*, 371–379. [[CrossRef](#)]
32. Chen, G.X.; Liang, K.; Zhao, K.; Yang, J. Shear modulus and damping ratio of saturated coral sand under generalised cyclic loadings. *Géotechnique*, **2022**; ahead of print. [[CrossRef](#)]
33. *ASTM D4253-14*; Standard Test Methods for Maximum Index Density and Unit Weight of Soils Using a Vibratory Table. ASTM International: West Conshohocken, PA, USA, 2006.
34. *ASTM D4254-14*; Standard Test Methods for Minimum Index Density and Unit Weight of Soils and Calculation of Relative Density. ASTM International: West Conshohocken, PA, USA, 2006.
35. *ASTM D2487*; Standard Practice for Classification of Soils for Engineering Purposes (Unified Soil Classification System). ASTM International: West Conshohocken, PA, USA, 2011.
36. Zhuang, H.Y.; Wang, R.; Chen, G.X.; Miao, Y.; Zhao, K. Shear modulus reduction of saturated sand under large liquefaction-induced deformation in cyclic torsional shear tests. *Eng. Geol.* **2018**, *240*, 110–122. [[CrossRef](#)]
37. Chen, G.X.; Ma, W.J.; Qin, Y.; Zhao, K.; Yang, J. Liquefaction susceptibility of saturated coral sand subjected to various patterns of principal stress rotation. *J. Geotech. Geoenviron. Eng.* **2021**, *147*, 04021093. [[CrossRef](#)]
38. Sze, H.Y.; Yang, J. Failure modes of sand in undrained cyclic loading: Impact of sample preparation. *J. Geotech. Geoenviron. Eng.* **2014**, *140*, 152–169. [[CrossRef](#)]
39. Huang, A.B.; Chang, W.J.; Hsu, H.H.; Huang, Y.J. A mist pluviation method for reconstituting silty sand specimens. *Eng. Geol.* **2015**, *188*, 1–9. [[CrossRef](#)]
40. *ASTM D5311D/5311M*; Standard Test Method for Load Controlled Cyclic Triaxial Strength of Soil. ASTM International: West Conshohocken, PA, USA, 2013.
41. Chen, G.X.; Zhou, Z.L.; Sun, T.; Wu, Q.; Xu, L.Y.; Sara, K.; Ling, D.S. Shear modulus and damping ratio of sand-gravel mixtures over a wide strain range. *J. Earthq. Eng.* **2019**, *23*, 1407–1440. [[CrossRef](#)]

42. Kumar, S.S.; Krishna, A.M.; Dey, A. Evaluation of dynamic properties of sandy soil at high cyclic strains. *Soil Dyn. Earthq. Eng.* **2017**, *99*, 157–167. [[CrossRef](#)]
43. Ghayoomi, M.; Suprunenko, G.; Mirshekari, M. Cyclic triaxial test to measure strain-dependent shear modulus of unsaturated sand. *Int. J. Geomech.* **2017**, *17*, 04017043. [[CrossRef](#)]
44. Wu, Q.; Hang, T.Z.; Zhao, K.; Chen, G.X. Reduction of dynamic shear modulus of saturated marine sandy silt under complex stress conditions. *Mar. Georesour. Geotech.* **2022**. [[CrossRef](#)]
45. Seed, H.B.; Wong, R.T.; Idriss, I.M.; Tokimatsu, K. Moduli and damping factors for dynamic analyses of cohesionless soils. *J. Geotech. Eng.* **1986**, *112*, 1016–1032. [[CrossRef](#)]
46. Yuan, X.M.; Sun, J.; Sun, R. Effect of Consolidation Ratios on Maximum Dynamic Shear Modulus of Sands. *Earthq. Eng. Eng. Vib.* **2005**, *4*, 59–68.
47. Sun, J.; Gong, M.S.; Tao, X.X. Dynamic shear modulus of undisturbed soil under different consolidation ratios and its effects on surface ground motion. *Earthq. Eng. Eng. Vib.* **2013**, *12*, 561–568. [[CrossRef](#)]
48. Hardin, B.O.; Drnevich, V. Shear modulus and damping in soils. *J. Soil Mech. Found. Div.* **1972**, *97*, 667–692. [[CrossRef](#)]
49. Yuan, X.M.; Sun, R.; Sun, J.; Meng, S.J.; Shi, Z.J. Laboratory experimental study on dynamic shear modulus ratio and damping ratio of soils. *Earthq. Eng. Eng. Vib.* **2000**, *20*, 133–139. [[CrossRef](#)]
50. Oztoprak, S.; Bolton, M.D. Stiffness of sands through a laboratory test database. *Geotechnique* **2013**, *63*, 54–70. [[CrossRef](#)]
51. Martin, P.P.; Seed, H.B. One-dimensional dynamic ground response analyses. *J. Geotech. Eng. Div.* **1982**, *108*, 935–952. [[CrossRef](#)]

Disclaimer/Publisher’s Note: The statements, opinions and data contained in all publications are solely those of the individual author(s) and contributor(s) and not of MDPI and/or the editor(s). MDPI and/or the editor(s) disclaim responsibility for any injury to people or property resulting from any ideas, methods, instructions or products referred to in the content.